CRYSTAL GROWTH & DESIGN

Article

Cite This: *Cryst. Growth Des.* 2018, 18, 5808−5815

pubs.acs.org/crystal

Real-Time Atomic Scale Observation of Surface-Induced Crystallization of a Bismuth Nanodroplet by Stepwise Ordering Mechanism

Yingxuan Li,*,† Mengmeng Huang,† Ling Zang,‡ Daniel L. Jacobs,‡ Jie Zhao,† Yunqing Zhu,† and Chuanyi Wang*,†

†School of Environmental Science and Engineering, Shaanxi University of Science and Technology, Xi'an 710021, China

‡Nano Institute of Utah and Department of Materials Science and Engineering, University of Utah, Salt Lake City, Utah 84112, United States

Supporting Information

ABSTRACT: Surface-induced crystallization of an isotropic Bi nanodroplet in three distinct steps was recorded at atomic resolution by *in situ* high resolution transmission electron microscopy. First, formation of a crystalline nucleus at the edge of the nanodroplet is induced by the liquid-state surface faceting, which initiates the formation of a prefreezing state with a distorted structure. Then, a periodic line pattern of the atomic columns with a periodicity of 0.49 nm that is relative to the interlayer spacing of the Bi crystal along the ⟨112⟩* direction (one-dimensional ordered structure) was formed by structure relaxation of the prefreezing nanoparticle, followed by a concerted growth and ordering process. Finally, the crystallization from the periodic structure was carried out by atom/atom interactions within and between the atomic layers to form the covalent Bi−Bi bonds that have the same arrangement as in the Bi crystal (crystallization along the ⟨1$\bar{1}$0⟩ direction). Motivated by the experimental observations, a stepwise ordering mechanism on the crystallization of a nanodroplet is revealed, which would provide new insight into the dynamics of phase transitions, crystal growth, and three-dimensional crystallization of supercrystals.

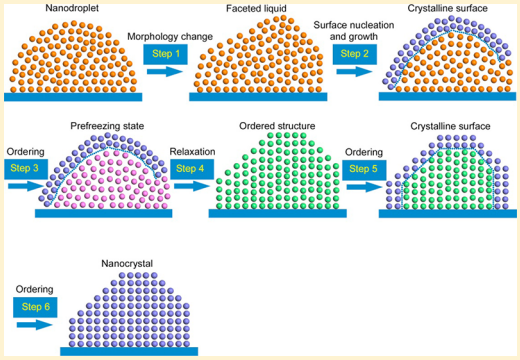

INTRODUCTION

Transformation of liquid into a solid crystal is a crucial issue in chemistry, and solid state physics, but also important for achieving fundamental understanding of the elusive mechanism of gelled states that are commonly observed in colloidal synthesis, and protein crystallization.[1−4] Classical nucleation theory (CNT) is widely adopted to describe the nucleation process of crystallization.[5] According to the CNT, the nucleation of a new phase depends on the competition between free energy gained from the phase transformation and the work needed for the formation of a surface.[5,6] As a result, the nucleation occurs only when the nucleus reaches a critical size, at which point the free energy is at a maximum. The crystallization process then proceeds through subsequent growth of critical nuclei throughout the liquid phase. Therefore, both nucleation and growth processes are crucial in driving the liquid transforming to the final solid phase.

In the nucleation processes of phase transitions, identifying the nucleation sites (within a particle or from the surface) is critical to studying the nucleation dynamics in the transitions.[7] Within the framework of CNT, the crystallization of a liquid should start at the center of the liquid, while melting for a single crystal should occur at the surface region.[8] The opposite effect of surface crystallization, i.e., a crystalline surface layers coexisting with its molten bulk, is rarely observed in experiments and simulations.[8−13] In colloidal systems and liquid crystals, surface-induced crystallization was induced because of the existence of anisotropic interactions between molecular chains.[13,14] In liquid metal and alloys, surface-induced crystallization has also been observed, including Hg, Ga, Sn, Bi−Sn, and Ga−In.[15−19] Recently, surface ordering was observed on metal−semiconductor alloys of $Au_{82}Si_{18}$ by X-ray study, which is related to the covalently bonded structure due to the segregation of Si atoms at the surface.[12] TEM observation has shown surface faceting of supercooled $Au_{72}Ge_{28}$ droplets, which provides an experimental evidence for surface-induced crystallization.[10] The occurrence of the surface-induced crystallization is mainly attributed to surface layering effects,[13] which are caused by a density oscillation near the surface. Although surface-induced nucleation has previously been evidenced by TEM imaging and X-ray study,[10,12] the microscopic dynamic and physical processes in the surface-induced crystallization remain poorly understood because no direct atomic-level observations on nucleation and the subsequent growth dynamics have been

Received: March 9, 2018
Revised: July 28, 2018
Published: August 20, 2018

DOI: 10.1021/acs.cgd.8b00370
Cryst. Growth Des. 2018, 18, 5808−5815

performed to explore how their structure evolves therein. Therefore, atomic scale observation on the crystallization dynamics from the earliest nucleation stage is needed for developing models for liquid−solid phase transitions that deviate from classical theory. However, the atomic scale observation remains a significant technical challenge at present because of the small size of nuclei and the fleeting and rare characteristics of the nucleation event.

Recently, the development of *in situ* transmission electron microscopy (TEM) has shown the potential to overcome this limitation with real-time, atomic scale visualization of electrochemical reactions,[20,21] nanoparticle growth,[22−25] biomaterials imaging,[26,27] phase transition,[28] nanocrystal etching,[29] etc. In our previous work,[30,31] the growth of Bi nanoparticles on a $SrBi_2Ta_2O_9$ platelet was induced by the electron-beam irradiation in a high resolution TEM (HRTEM). Simultaneously, the unique growth and phase transitions (mediated by prefreezing/premelting states) of Bi nanoparticles from the initial stages of nucleation have been studied by the HRTEM, which shows a potential to study the atomic mechanism in nanoparticle growth and phase transitions. Furthermore, lattice and coalescence induced nucleation and growth were also observed in the Bi-based systems by using aberration corrected TEM.[32−35] In this work, the nucleation and growth of Bi nanoparticles on a $SrBi_2Ta_2O_9$ platelet was quantitatively analyzed through *in situ* HRTEM to reveal a surface-induced crystallization pathway through a stepwise ordering mechanism. For the first time, it provides a valuable platform for *in situ* studying the initial nucleation and growth dynamics of the surface-induced crystallization mechanism of the nanodroplets in atomic scale.

EXPERIMENTAL SECTION

Sample Preparation. $SrBi_2Ta_2O_9$ was synthesized by a molten salt, in which the mixture of NaCl and KCl (1:1 molar ratio) was used as molten salt.[30,31,36] The starting materials ($Sr(NO_3)_2$, Bi_2O_3, and Ta_2O_5) were weighed according to the composition of $SrBi_2Ta_2O_9$ and then mixed with the molten salts (in weight ratio 1:1) by grinding in an agate mortar. After 0.5 h grinding, the mixture was transferred into an alumina crucible and heated at 850 °C for 3 h. The obtained product was washed with deionized water to remove the chlorides and finally dried at 50 °C for 3 h.

HRTEM Observation. The formation and phase transition of Bi nanoparticles were achieved by electron-beam irradiation on a $SrBi_2Ta_2O_9$ platelet in the TEM (JEOL model JEM-2100), which was operated at an accelerating voltage of 200 keV. Simultaneously, the phase transition trajectory was recorded as a video in atomic scale using a CCD camera (Gatan 832). Energy-dispersive X-ray spectroscopy was recorded on the FEI Tecnai F30 electron microscope after the $SrBi_2Ta_2O_9$ sample was irradiated by an electron beam for 20 min, at which Bi nanoparticles have been formed.

RESULTS

Formation of Crystalline Surface in the Nanodroplet. The formation of pure metallic Bi (nanodroplets or nanocrystals) on the $SrBi_2Ta_2O_9$ by electron-beam irradiation was confirmed by energy dispersive spectroscopy analysis (EDS). As shown in Figure 1, the EDS result clearly reveals that the nanoparticle is composed of elemental Bi, which is consistent with the previous report.[30−33] The signals of carbon and copper in Figure 1 are derived from the carbon-coated copper grid.

Here, electron-beam irradiation was used to form Bi nanodroplets on the surface of a $SrBi_2Ta_2O_9$ solid. When the size of the nanodroplet reached to a critical size, continued

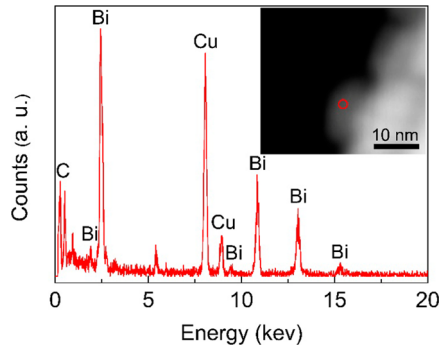

Figure 1. EDS spectrum of the single Bi nanoparticle anchored to the edge of a $SrBi_2Ta_2O_9$ platelet, as marked by the red circled region in the high-angle annular dark-field scanning transmission electron microscopy (HAADF-STEM) image (the inset).

irradiation caused crystallization of the Bi nanodroplets. The crystallization process was recorded as a real-time video as shown in Video S1, which was recorded between 1056 and 1092 s after TEM beam irradiation. The nanoparticle we studied is the one marked in the rectangle in Video S1. Before crystallization, frequent surface oscillations of the nanoparticle are clearly shown in Video S1, which indicates the liquid nature of the nanoparticle.[31] TEM snapshots of the nucleation process are shown in Figure 2. The initial state of the nanoparticle is liquid as

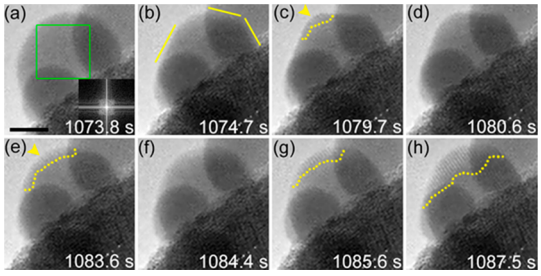

Figure 2. (a−h) Sequential snapshots of HRTEM images showing surface nucleation dynamics in the crystallization of a Bi nanodroplet. The inset of (a) shows the corresponding FFT pattern of the region as marked by the square. The solid yellow lines in (b) mark extended planar surface facets. The yellow arrows in (c) and (e) indicate the small nucleation before the critical size, which keeps dynamic transformation between liquid and solid phase. The boundaries between liquid and solid are marked by the dashed yellow lines. The scale bar is 5 nm, which applies to all the HRTEM images.

confirmed by the fast Fourier transform (FFT) pattern in Figure 2a.[31] At 1074.7 s, this liquid droplet was converted from a rounded surface to the one with multiple planar facets as highlighted by the yellow lines in Figure 2b. Following this shape change, the nanodroplet entered a state where rapid formation and dissolution of small crystallized clusters occurred along the outer surface of the droplet Figure 2c−f. This observation resembles the classical nucleation model, where crystalline embryos fluctuate their sizes before reaching a critical nucleus size. The lattice spacing of the ordered phase in the surface region is about 0.40 nm (Figure 2e), which corresponds to the *d*-spacing of the (003) lattice of a Bi crystal. After the induction period, the final crystalline nucleus was formed at 1085.6 s as outlined by the yellow dotted line in Figure 2g. After nucleation, the growth of the critical nucleus by monomer attachment is observed in Video S1 and Figure 2h, indicating that the classical

DOI: 10.1021/acs.cgd.8b00370
Cryst. Growth Des. 2018, 18, 5808−5815

growth model plays a role in the growth process. Formation of a planar surface on a droplet (Figure 2b) is not a common phenomenon as it requires an anisotropic distribution of surface free energy, which does not exist in pure liquid phase. This suggests that the observed liquid−solid phase transition in the present work is primarily based on a surface-induced nucleation mechanism.[10] Although surface-induced nucleation has previously been evidenced by TEM imaging,[10] this is the first atomic-level imaging on this process from the earliest stage of nucleation.

Formation of Periodic Structure in One Direction in the Nanoparticle. As shown in Figure 3a, an ordered piece of the crystallized phase along the outer surface of the nanodroplet is formed by the surface nucleation and growth. The phase boundary between liquid and solid phases can be clearly observed in Figure 3a (highlighted by the yellow line). As shown in Figure 3a, the depth of the crystallized layer reaches ∼2 nm (8−9 well-defined atomic layers), which is comparable with the AuSi alloy.[12] As shown in Figure 3b−d, the crystalline surface layer does not grow toward the interior; instead, the phase boundary serves as an effective substrate to stimulate heterogeneous nucleation and formation of a solid-like phase with a distorted structure (Figure 3d). The observed disordered structure can be regarded as prefreezing of the nanodroplet similar to our previous observation.[31] The FFT pattern in Figure 3d shows that the disordered structure shares the same crystal direction with the crystallized surface, implying that the formation of the prefreezing state inside the drop may originate from the surface. However, as shown in the following, the real crystallization trajectory after the formation of the prefreezing state is far beyond the simplified one-step process as observed in our previous report.[31]

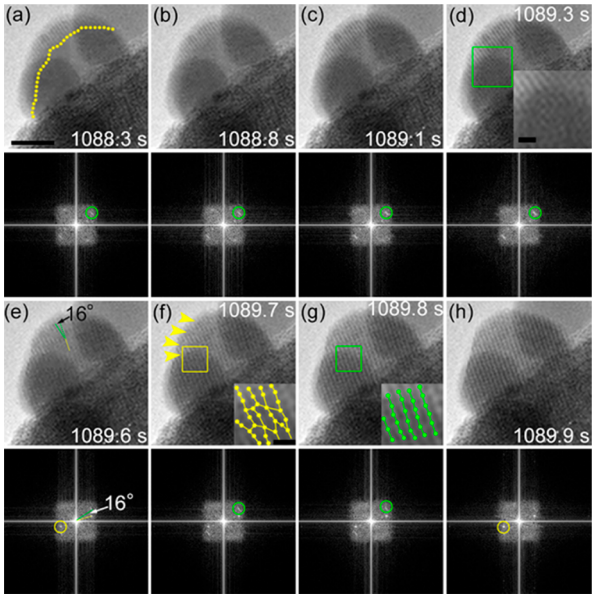

Figure 3. (a−h) Sequential snapshots of HRTEM images showing formation trajectory of the periodic structure in one direction after the first surface-induced nucleation. The boundary between liquid and solid in (a) is marked by the dashed yellow line. The corresponding FFT patterns of the nanoparticles are shown below the HRTEM images. The spots marked by the green and yellow circles correspond to the lattice with *d*-spacing of 0.40 and 0.49 nm, respectively. For clarity, the enlarged images of the regions as marked by the green and yellow squares in (d), (f), and (g) are displayed, and some lattice fringes and atoms in (f) and (g) are highlighted. The yellow arrows in (f) indicate the directions in which the dislocations are observed clearly. The scale bar in (a) is 5 nm, which applies to all the HRTEM images. The scale bars in the insets of (d) and (f) are 1 nm. The scale bar in the inset of (f) can also apply to the inset image of (g).

A significant change occurred at 1089.6 s (Figure 3e), at which the nanoparticle abruptly relaxed to an intermediate state with the intergrowth of solid-like layers and liquid-like layers. Carefully analyzing the fast Fourier transformation (FFT) pattern in Figure 3e, it is noted that, other than the spots corresponding to the crystal nucleus lattice shown in Figure 3a, an additional weak spot (arrowed) corresponding to the *d*-spacing of 0.49 nm appears, which should originate from the newly formed solid-like phase after sudden transformation. As shown in Figure 3e, the two different lattices are aligned with a small-angle (about 16°) mismatch. The fast relaxation of the nanoparticle in Figure 3d,e implies that this transformation is different from the traditional nucleation and growth process, but decomposes throughout the entire system, indicating that this process might proceed via a massive transformation mechanism.[37] In the massive mechanism, a phase transformation is taking place by diffusional nucleation and growth.[38] Following this mechanism, the disordered state in Figure 3d is rearranged into another metastable state (Figure 3e) by the fast atomic displacement at an angstrom scale.

As shown in Figure 3e−h, further growth of the ordered structure occurs by consuming the isolated liquid-like layers. Simultaneously, the planes with 0.40 nm *d*-spacing are gradually transformed and fuse with the planes with 0.49 nm *d*-spacing via a continuous rotation and reconstruction process as confirmed by the HRTEM images and FFT patterns in Figure 3e−h. The reconstructed lattice image from the outlined area in Figure 3f clearly shows the existence of partial dislocation in the interface of the two adjacent regions, indicating that the fusion process of the crystallized clusters follows the oriented attachment mechanism.[39] Some other dislocations can also be found along the directions indicated by the yellow arrows in Figure 3f. The continued flattening of the protruded dislocations is observed in Figure 3f−h. To clarify the restructuring of the nanoparticle and flattening of the partial dislocation during this process, the regions marked by the rectangles in panels (f) and (g) in Figure 3 are enlarged at the lower right of each image. The appearance of diffraction spots in the FFT patterns and the clearer development of the lattice fringe in Figure 3e−h suggest the improvement in the ordering of the nanoparticle. As a result, the nanoparticle composed of a periodic line pattern of the atomic columns with a periodicity of 0.49 nm was formed at 1089.9 s (Figure 3h), which is assigned to the interlayer spacing of the Bi crystal along the ⟨112⟩* direction (0.475 nm).[40] On the basis of the *in situ* observation, it can be concluded that the periodic structure is formed by a concerted growth and ordering process, which has never been directly observed previously in atomic scale. In the ordering process, the initial curved edge morphology of the nanoparticle in Figure 3a gradually transforms to a faceted configuration that is atomically sharp (Figure 3h). The overall change in the shape can be attributed to the motion of interior atoms along a transition path.[41] However, from the HRTEM image and the corresponding FFT pattern in Figure 3h, we can find that the atoms in the same planes with 0.49 nm *d*-spacing are randomly oriented. This observation indicates that the nanoparticle shown in Figure 3h is a periodic structure in one direction that is constituted by organized two-dimensional (2D) atomic layers, implying that further ordering

DOI: 10.1021/acs.cgd.8b00370
Cryst. Growth Des. 2018, 18, 5808−5815

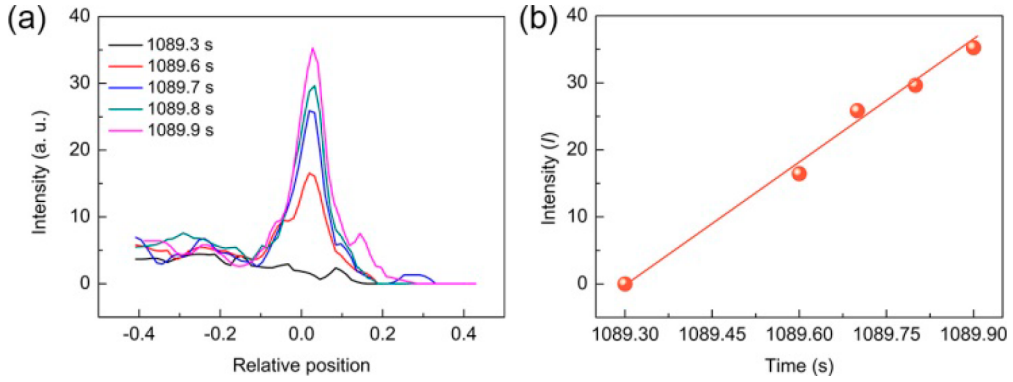

Figure 4. (a) The integrated profiles taken from the 2D FFT images in Figure 2d–h. The peaks correspond to the diffraction spots indicated by the yellow circles. (b) The peak intensity corresponding to the different timing shown in (a).

of the atoms is needed for the complete crystallization of the nanoparticle.

In order to study the ordering process in Figure 3 quantitatively, the FFT spots (corresponding to the atomic layers with 0.49 nm *d*-spacing) were integrated into 1D data (Fourier spectra) according to our previous reports using the Fit2D program (Figure 4a).[31,42] As shown in Figure 4b, the intensity (I) of the Fourier spectra increases linearly with time right after the initial ordering, which implies that the ordering process is continuous.

Crystallization of the Nanoparticle from the Periodic Structure. The continued crystallization process occurs through the atomic arrangement within the atomic planes that constitute the 3D nanostructure. The nanoparticle in Figure 5a

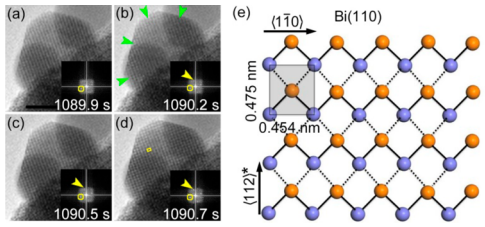

Figure 5. (a–d) Sequential snapshots of HRTEM images showing the crystallization process of the periodic structure formed after the first nucleation and growth process. The corresponding FFT patterns of the nanoparticle are shown in the insets of the HRTEM images. In the FFT image, the spots marked by the yellow circles correspond to the lattice with *d*-spacing of 0.49 nm, while the spots indicated by yellow arrows correspond to the lattice with *d*-spacing of 0.45 nm. The green arrows in (b) indicate the crystalline nuclei along the outer surface of the nanoparticle. The scale bar is 5 nm, which applies to all the HRTEM images. (e) Schematic showing top view of the Bi(110) surface with the two atom unit cell shaded. Atoms in purple and orange represent the 1st and 2nd layer, respectively. Solid lines indicate the strong covalent bonds, and dashed lines represent the weaker interlayer bonds.

is identical to that in Figure 3h. As shown in Figure 5, the atom/atom interactions in the nanoparticle lead to the further ordering of atomic lattices along the orthogonal direction of $\langle 1\bar{1}0\rangle$ to form a higher-order structure. As a result, a new set of diffraction spots corresponding to the lattice space of 0.45 nm clearly appears in the FFT pattern in Figure 5d (indicated by the yellow arrows). In this reorganization process, the *d*-spacing of 0.49 nm along the $\langle 112\rangle^*$ direction is maintained throughout as indicated in the yellow circles in the FFT patterns. As shown by the HRTEM image in Figure 5d, the final phase has a crystallographic structure that is the same as the regular arrangement of atoms in the Bi crystal orientated with the (110) facet. As shown in Figure 5b and Video S1, the ordering process along the $\langle 1\bar{1}0\rangle$ direction also proceeds from the surface toward the core region of the nanoparticle (more details of dynamic change shown in Video S1), finally leading to a crystalline structure of Bi (Figure 4d).

The atomic structure of the bulk Bi(110) surface is shown in Figure 5e, which is characterized by a unit cell of 0.454 nm × 0.475 nm containing two Bi atoms.[43] In Figure 5d, a representative unit cell is highlight by yellow lines. The dimensions of the surface unit cell were estimated to be 0.45 nm × 0.49 nm by the FFT analysis of the image (inset of Figure 5d). The first number (0.45 nm) is consistent with the bulk interatomic separation (0.454 nm) along the $\langle 1\bar{1}0\rangle$ direction of a rhombohedral Bi structure, while the other one is larger than that in the bulk (0.475 nm) along the $\langle 112\rangle^*$ direction.[43] The expansion of the Bi(110) surface unit cell along the $\langle 112\rangle^*$ direction has also been reported previously, which is related to the layered feature of a Bi crystal along this direction.[44] As shown in Figure 5e, the atoms of the Bi crystal are arranged in bilayers, which could also be viewed as a single puckered layer. This crystal orientation is characterized by long zigzag chains of covalent bonds in the $\langle 1\bar{1}0\rangle$ direction (solid lines), separated by the van der Waals (vdW)-type interlayer bonds in the orthogonal direction $\langle 112\rangle^*$ (dashed lines), which is similar to the ordinary layered crystals, such as graphite. The expansion of the unit cell in the $\langle 112\rangle^*$ direction is due to stretching of weak vdW bonds.[44] However, it is much more difficult to expand the lattice in the $\langle 1\bar{1}0\rangle$ direction than in the $\langle 112\rangle^*$ direction because of the existence of the stronger covalent bonds.[44] Therefore, the interatomic separation along the $\langle 1\bar{1}0\rangle$ direction agrees with that in the bulk (0.454 nm).

The final ordering process in crystallization of the nanoparticle can be quantified by calculating the crystalline order of the entire nanoparticle along the $\langle 1\bar{1}0\rangle$ direction that is reflected by the intensity of the integrated profile of the FFT spot. The intensity profiles (corresponding to the FFT spot of 0.45 nm *d*-spacing) and the evolution of the peak intensity with time in the ordering process are shown in Figure 6a,b, respectively. As shown in Figure 6b, there is no obvious change in the crystalline order between 1089.9 and 1090.5 s. However, an abrupt increase in the peak intensity is observed after nucleation (at 1090.7 s), indicating that the structural change occurs discontinuously in the crystallization process as shown in Figure 5a–d.

DOI: 10.1021/acs.cgd.8b00370
Cryst. Growth Des. 2018, 18, 5808–5815

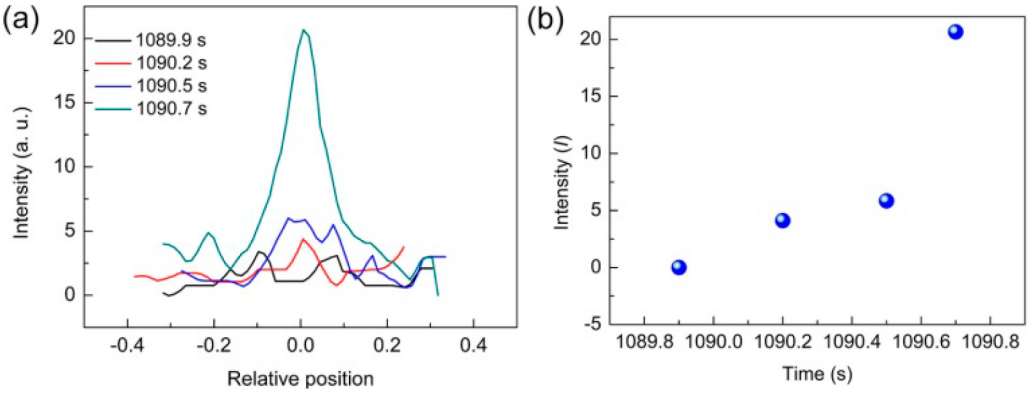

Figure 6. (a) The integrated profiles taken from the 2D FFT images in Figure 4a–d. The peaks correspond to the diffraction spots indicated by the yellow arrows. (b) The peak intensity corresponding to the different timing shown in (a).

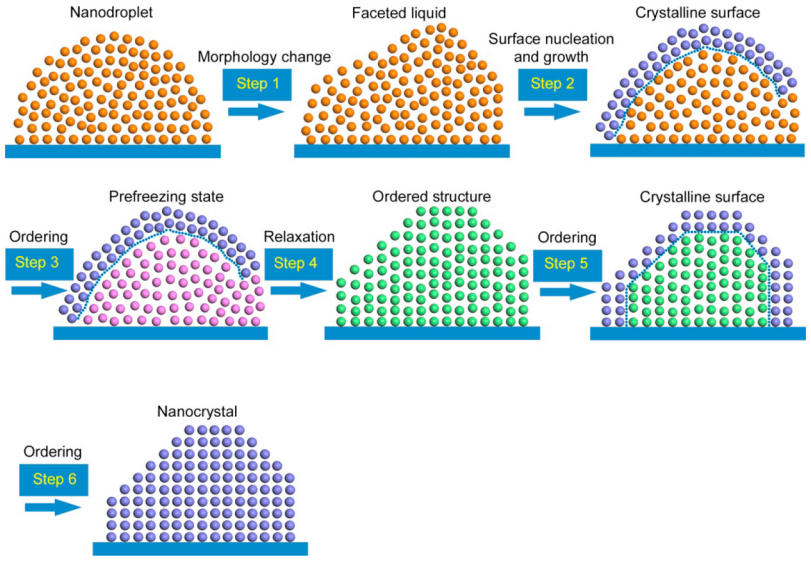

Figure 7. Schematic illustration of crystallization pathways initiated from surface faceting. The spheres represent the atoms in the nanoparticle. The colors represent different states. Orange, purple, magenta, and green represent liquid state, crystalline phase, distorted structure, and 1D ordered structure, respectively. The crystalline surface is outlined by the dashed blue lines.

DISCUSSION

Theoretically, the crystallization of a liquid can proceed by either volume or surface nucleation model.[9] Recently, on the basis of the experimental results, Tabazadeh and co-authors predict that micrometer water droplets can homogeneously crystallize into ice by a surface-induced nucleation mechanism.[9] On the basis of the model proposed by Tabazadeh et al., the total nucleation rate (J) per unit time and unit volume is determined by volume (J_V)- and surface (J_S)-dominated nucleation rates

$$J = J_V V_T + J_S S_T \quad (1)$$

where V_T and S_T are the total volume and surface area of the droplet, respectively. The classical volume-based nucleation can be used only when $J_V V_T \gg J_S S_T$. For the nanodroplet with large surface-to-volume ratios, the second term in eq 1 may play a more prominent role in nucleation; thus a surface-dominated crystallization might be observed in the nanodroplet.

In addition to the size effect, the high surface mobility of the Bi nanodroplet observed in Video S1 might be the other factor inducing the surface-dominated crystallization, which has been found as a dominant factor for the surface-induced crystallization of metallic glass.[45] The surface crystallization process can create an interface between the crystal-like and the liquid-like structures, which in turn accelerates the following transformation. Therefore, in the heterogeneous system, the high dynamic mobility in the Bi nanodroplet might be the other reason for the surface crystallization as in the case of the present experiments, rather than the interfacial crystallization. As reported previously, the phase transitions in the Bi nanoparticle are nonlocal behaviors.[31,34] Therefore, the local surface crystallization behavior and the cooperative multiscale interaction in the Bi nanoparticle might contribute to the crystallization pathway observed in the present experiments that is similar to the homogeneous system.

Our *in situ* HRTEM observations suggest a possible pathway for the crystallization of liquid, and the main processes of the surface-induced crystallization are schematically illustrated in Figure 7. As shown in Figure 7, formation of a crystalline nucleus at the edge of the nanodroplet is induced by the liquid-state surface faceting (Step 1). Nucleus growth takes place along the outer surface of the droplet, leading to the formation of a "crystal cap" on the nanoparticle (Step 2). Compared with the crystal nucleation in the core region of the droplet, forming a faceted liquid surface would reduce the free energy barrier for nucleation as discussed in the following. The role of a faceted liquid surface

DOI: 10.1021/acs.cgd.8b00370
Cryst. Growth Des. 2018, 18, 5808–5815

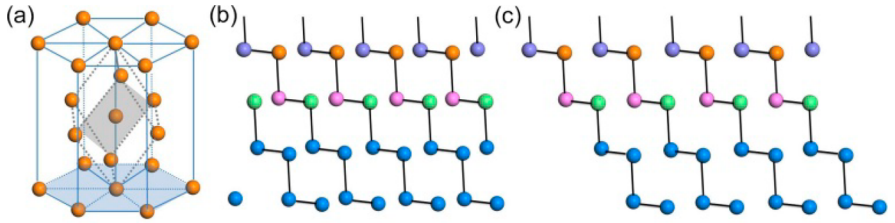

Figure 8. (a) A schematic of the bulk Bi crystal structure. The Bi(111) plane is shaded with blue color. The Bi(110) plane is shaded with gray color. (b and c) Models for surface planes of ideal Bi crystal viewed in the ⟨112⟩* direction and ⟨1$\bar{1}$0⟩ direction, respectively. Atoms in different layers are indicated using different colors: purple, orange, magenta, and green for 1st, 2nd, 3rd, and 4th layer, respectively.

(Figure 2b) in the surface-induced crystallization of a liquid can be described by a previously reported model.[13] Starting from CNT, the nucleation rate is given by

$$R = A \exp(-\Delta G_{crit}/k_B T) \quad (2)$$

where k_B is the Boltzmann's constant, A is the pre-exponential factor dependent on diffusion, and ΔG_{crit} is the nucleation free energy barrier of the critical nucleus. The probability for the formation of a critical nucleus depends on A and ΔG_{crit}. The free-energy change in the nucleation process, ΔG, is determined by both the solid−liquid interface energy ΔG_i and volume free energy change ΔG_v

$$\Delta G_1 = \Delta G_i + \Delta G_v \quad (3)$$

As shown in Figure 2, the planar facets observed on the liquid droplet would produce a small lateral pressure in the facet ($p < 0$, parallel to the surface). Thus, a pressure-dependent term, $\delta G_v(p)$, must be added to ΔG_v[13]

$$\delta G_v(p) = \frac{\lambda p(\rho_L - \rho_S)}{\rho_L \rho_S} \quad (4)$$

where λ is the number of atoms in the nucleation cluster, ρ_L and ρ_S are the mass densities of the liquid and solid state, respectively. Solid Bi has a lower density of 9.649 g/cm^3 at the melting temperature compared to that of liquid Bi (10.050 g/cm^3),[46] which results in a negative value of $\delta G_v(p)$ according to eq 4, thus lowering the value of ΔG_v compared with bulk nucleation. The value of ΔG_i in surface nucleation is similar to that in bulk nucleation.[13] As a result, the nucleation barrier (ΔG_{crit}) near the liquid facet in Figure 2 is decreased compared with that in the bulk. Therefore, the nucleation of the crystal preferentially occurred in the surface region as observed in Figure 2. Subsequently, the arrangement of lattice planes along the ⟨112⟩* direction of the Bi crystal is achieved gradually by continuous rotation and interaction of the ordered lattices (Step 4).

The final ordering also occurs from the surface region of the periodic structure through a building up of atoms according to the symmetry of the Bi crystal (Step 5), which is followed by the fast ordering of the atoms along the ⟨1$\bar{1}$0⟩ direction (Step 6). In Steps 5 and 6, vdW force between the atomic layers is important in maintaining the periodicity of the lattice planes along the ⟨112⟩* direction. In this process, atom/atom interactions within the individual layers and between the adjacent layers lead to the formation of the Bi−Bi bonds (covalent bonds) and the modifications of the atoms at angstrom scale over the whole nanoparticle, which allows the atoms to self-order to 3D regular arrangement of Bi with (110)-orientation (shaded with gray color in Figure 8a) to complete the crystallization of the nanodroplet. The atom moving from one position to an equivalent adjacent position relative to the Bi lattice geometry is caused by a very delicate balance between in-plane and interplane forces. In the crystallization trajectory, each step of the transition follows a group-subgroup relation based on symmetry, and the intermediate states bridge the parent and the product phases. In comparison with the previous multistep crystallization,[47,48] the experimental observations in the present work are remarkable because the Bi crystal has angstrom-scale lattice parameters and the similar dynamic pathways of the crystallization processes have never been directly observed previously. However, in order to quantitatively understand the multistep nucleation in crystallization, computer simulations are suggested to calculate the quantitative energy variations in the formation of each intermediate phase.

As shown in the atomic models viewed from the ⟨112⟩* direction (Figure 8b) and ⟨1$\bar{1}$0⟩ direction (Figure 8c), the interatomic distance along the perpendicular direction of the HRTEM image is determined by the Bi−Bi covalent bonds. As shown in Figure 5b−d, the formation of the Bi−Bi covalent bonds occurs between 1090.2 and 1090.7 s, indicating that the ordering of atoms along the perpendicular direction of the HRTEM image may occur at this stage. The precise determination of the three-dimensional atomic structure of the nanoparticle from a single HRTEM image remains challenging because of the lacking of the out-of-plane resolution. Therefore, a description of the structure along the perpendicular direction of the HRTEM image cannot proceed. However, this uncertainty does not prohibit us to come to the conclusion on the multistep nucleation mechanism in crystallization of a liquid.

From a statistical standpoint, not all of the nanoparticles activated by electron-beam irradiation in HRTEM are predicted to show identical trajectories and transition rates because of the effects by the instrument and the size of the sample.[37] In a previous report, we have found that the crystalline nucleus in the crystallization of the nanodroplet is directly formed from liquid phase.[31] However, the present crystallization pathway of the Bi nanodroplet is significantly different to our previous finding. It should be indicated that the two crystallization processes were acquired under the same conditions. Therefore, the different crystallization pathways do not result from the effect of the experimental conditions. It is speculated that the two different transition mechanisms observed are determined by the crystal habit of the solid phase considering that the final nanocrystal in the present work is (110)-orientated, while it is (111)-orientated in our previous report. As shown in Figure 8a, a (111) plane and a (110) plane are shaded in blue and gray colors, respectively. This structure dependent crystallization provides a platform for isolating and measuring new metastable phases in liquid−solid phase transitions. Our results also indicate that the liquid−solid phase transitions are not always carried out along the same fixed pathway, even under the same experimental conditions. This

DOI: 10.1021/acs.cgd.8b00370
Cryst. Growth Des. 2018, 18, 5808−5815

highlights the extreme dependence of the state of the system on the crystallization process and why various freezing processes can be observed in nature. Statistical investigations accompanied by quantitative simulations should be considered in the future studies to further understand the surface-induced crystallization by a stepwise ordering mechanism.

CONCLUSION

The *in situ* HRTEM observations conclusively demonstrate that the crystallization of the nanodroplet is completed by a stepwise ordering mechanism through stepwise arrangement of the atomic lattices throughout the entire nanoparticle according to the layered structure of the final Bi nanocrystal. In contrast to the conventional understanding that the crystallization of a liquid should start at the center of the liquid, we observed that the crystallization was initiated by a precursor of liquid-state surface faceting, followed by a surface-induced crystallization. Our observation also reveals a precursor (a periodic line pattern of the atomic columns) of crystalline nuclei in crystallization of the nanodroplet that was not previously observed. The unusual crystallization process is helpful in refining the theories for nucleation, growth, and transformation behaviors in liquid−solid phase transitions. Furthermore, the recognition of intermediate states before the nucleation by our atomic scale imaging will provide new insight into understanding transformation dynamics from prenucleation stages, which is the first crucial step for controlling phase transition behaviors.

ASSOCIATED CONTENT

Supporting Information

The Supporting Information is available free of charge on the ACS Publications website at DOI: 10.1021/acs.cgd.8b00370.

Video S1: Real-time HRTEM imaging of motion of crystallization of a Bi nanodroplet induced by electron-beam irradiation, indicating a novel multistep crystallization mechanism (AVI)

AUTHOR INFORMATION

Corresponding Authors

*E-mail: liyingxuan@sust.edu.cn (Y.L.).
*E-mail: wangchuanyi@sust.edu.cn (C.W.).

ORCID

Yingxuan Li: 0000-0002-9139-4177

Notes

The authors declare no competing financial interest.

ACKNOWLEDGMENTS

This work was supported by the National Natural Science Foundation of China (Grant Nos. 21643012 and U1403193).

REFERENCES

(1) Jacobson, L. C.; Molinero, V. Can Amorphous Nuclei Grow Crystalline Clathrates? The Size and Crystallinity of Critical Clathrate Nuclei. *J. Am. Chem. Soc.* **2011**, *133*, 6458−6463.

(2) Gasser, U.; Weeks, E. R.; Schofield, A.; Pusey, P. N.; Weitz, D. A. Real-Space Imaging of Nucleation and Growth in Colloidal Crystallization. *Science* **2001**, *292*, 258−262.

(3) Savage, J. R.; Dinsmore, A. D. Experimental Evidence for Two-Step Nucleation in Colloidal Crystallization. *Phys. Rev. Lett.* **2009**, *102*, 198302.

(4) Vekilov, P. G. Nucleation. *Cryst. Growth Des.* **2010**, *10*, 5007−5019.

(5) Erdemir, D.; Lee, A. Y.; Myerson, A. S. Nucleation of Crystals from Solution: Classical and Two-Step Models. *Acc. Chem. Res.* **2009**, *42*, 621−629.

(6) Vivares, D.; Kaler, E. W.; Lenhoff, A. M. Quantitative Imaging by Confocal Scanning Fluorescence Microscopy of Protein Crystallization *via* Liquid−Liquid Phase Separation. *Acta Crystallogr., Sect. D: Biol. Crystallogr.* **2005**, *61*, 819−825.

(7) Mendez-Villuendas, E.; Bowles, R. K. Surface Nucleation in the Freezing of Gold Nanoparticles. *Phys. Rev. Lett.* **2007**, *98*, 185503.

(8) Nam, H.-S.; Hwang, N. M.; Yu, B. D.; Yoon, J.-K. Formation of an Icosahedral Structure During the Freezing of Gold Nanoclusters: Surface-Induced Mechanism. *Phys. Rev. Lett.* **2002**, *89*, 275502.

(9) Tabazadeh, A.; Djikaev, Y. S.; Reiss, H. Surface Crystallization of Supercooled Water in Clouds. *Proc. Natl. Acad. Sci. U. S. A.* **2002**, *99*, 15873−15878.

(10) Sutter, P. W.; Sutter, E. A. Dispensing and Surface-Induced Crystallization of Zeptolitre Liquid Metal-Alloy Drops. *Nat. Mater.* **2007**, *6*, 363−366.

(11) Nielsen, M. H.; Aloni, S.; De Yoreo, J. J. *In Situ* TEM Imaging of $CaCO_3$ Nucleation Reveals Coexistence of Direct and Indirect Pathways. *Science* **2014**, *345*, 1158−1162.

(12) Shpyrko, O. G.; Streitel, R.; Balagurusamy, V. S. K.; Grigoriev, A. Y.; Deutsch, M.; Ocko, B. M.; Meron, M.; Lin, B.; Pershan, P. S. Surface Crystallization in a Liquid AuSi Alloy. *Science* **2006**, *313*, 77−80.

(13) Li, T.; Donadio, D.; Ghiringhelli, L. M.; Galli, G. Surface-Induced Crystallization in Supercooled Tetrahedral Liquids. *Nat. Mater.* **2009**, *8*, 726−730.

(14) Lang, P. Surface Induced Ordering Effects in Soft Condensed Matter Systems. *J. Phys.: Condens. Matter* **2004**, *16*, R699−R720.

(15) Magnussen, O. M.; Ocko, B. M.; Regan, M. J.; Penanen, K.; Pershan, P. S.; Deutsch, M. X-Ray Reflectivity Measurements of Surface Layering in Liquid Mercury. *Phys. Rev. Lett.* **1995**, *74*, 4444−4447.

(16) Regan, M. J.; Kawamoto, E. H.; Lee, S.; Pershan, P. S.; Maskil, N.; Deutsch, M.; Magnussen, O. M.; Ocko, B. M.; Berman, L. E. Surface Layering in Liquid Gallium: An X-Ray Reflectivity Study. *Phys. Rev. Lett.* **1995**, *75*, 2498−2501.

(17) Shpyrko, O. G.; Grigoriev, A. Y.; Steimer, C.; Pershan, P. S.; Lin, B.; Meron, M.; Graber, T.; Gerbhardt, J.; Ocko, B.; Deutsch, M. Anomalous Layering at the Liquid Sn Surface. *Phys. Rev. B: Condens. Matter Mater. Phys.* **2004**, *70*, 224206.

(18) Shpyrko, O. G.; Grigoriev, A. Y.; Streitel, R.; Pontoni, D.; Pershan, P. S.; Deutsch, M.; Ocko, B.; Meron, M.; Lin, B. Atomic-Scale Surface Demixing in a Eutectic Liquid BiSn Alloy. *Phys. Rev. Lett.* **2005**, *95*, 106103.

(19) González, D. J.; González, L. E. Structure of the Liquid−Vapor Interfaces of Ga, In and the Eutectic Ga−In Alloy—an ab initio Study. *J. Phys.: Condens. Matter* **2008**, *20*, 114118.

(20) Williamson, M. J.; Tromp, R. M.; Vereecken, P. M.; Hull, R.; Ross, F. M. Dynamic Microscopy of Nanoscale Cluster Growth at the Solid−Liquid Interface. *Nat. Mater.* **2003**, *2*, 532−536.

(21) White, E. R.; Singer, S. B.; Augustyn, V.; Hubbard, W. A.; Mecklenburg, M.; Dunn, B.; Regan, B. C. *In Situ* Transmission Electron Microscopy of Lead Dendrites and Lead Ions in Aqueous Solution. *ACS Nano* **2012**, *6*, 6308−6317.

(22) Zheng, H.; Smith, R. K.; Jun, Y. W.; Kisielowski, C.; Dahmen, U.; Alivisatos, A. P. Observation of Single Colloidal Platinum Nanocrystal Growth Trajectories. *Science* **2009**, *324*, 1309−1312.

(23) Kimura, Y.; Niinomi, H.; Tsukamoto, K.; García-Ruiz, J. M. *In Situ* Live Observation of Nucleation and Dissolution of Sodium. *J. Am. Chem. Soc.* **2014**, *136*, 1762−1765.

(24) Yuk, J. M.; Park, J.; Ercius, P.; Kim, K.; Hellebusch, D. J.; Crommie, M. F.; Lee, J. Y.; Zettl, A.; Alivisatos, A. P. High-Resolution EM of Colloidal Nanocrystal Growth Using Graphene Liquid Cells. *Science* **2012**, *336*, 61−64.

(25) Liao, H.-G.; Zherebetskyy, D.; Xin, H.; Czarnik, C.; Ercius, P.; Elmlund, H.; Pan, M.; Wang, L.-W.; Zheng, H. Facet Development During Platinum Nanocube Growth. *Science* **2014**, *345*, 916−919.

DOI: 10.1021/acs.cgd.8b00370
Cryst. Growth Des. 2018, 18, 5808−5815

(26) Jonge, N.; Peckys, D. B.; Kremers, G. J.; Piston, D. W. Electron Microscopy of Whole Cells in Liquid with Nanometer Resolution. *Proc. Natl. Acad. Sci. U. S. A.* **2009**, *106*, 2159−2164.
(27) Peckys, D. B.; Veith, G. M.; Joy, D. C.; de Jonge, N. Nanoscale Imaging of Whole Cells Using a Liquid Enclosure and a Scanning Transmission Electron Microscope. *PLoS One* **2009**, *4*, e8214.
(28) Zheng, H.; Rivest, J. B.; Miller, T. A.; Sadtler, B.; Lindenberg, A.; Toney, M. F.; Wang, L.-W.; Kisielowski, C.; Alivisatos, A. P. Observation of Transient Structural-Transformation Dynamics in a Cu_2S Nanorod. *Science* **2011**, *333*, 206−209.
(29) Jiang, Y.; Zhu, G.; Lin, F.; Zhang, H.; Jin, C.; Yuan, J.; Yang, D.; Zhang, Z. *In Situ* Study of Oxidative Etching of Palladium Nanocrystals by Liquid Cell Electron Microscopy. *Nano Lett.* **2014**, *14*, 3761−3765.
(30) Li, Y.; Bunes, B. R.; Zang, L.; Zhao, J.; Li, Y.; Zhu, Y.; Wang, C. Atomic Scale Imaging of Nucleation and Growth Trajectories of an Interfacial Bismuth Nanodroplet. *ACS Nano* **2016**, *10*, 2386−2391.
(31) Li, Y.; Zang, L.; Jacobs, D. L.; Zhao, J.; Yue, X.; Wang, C. *In Situ* Study on Atomic Mechanism of Melting and Freezing of Single Bismuth Nanoparticles. *Nat. Commun.* **2017**, *8*, 14462.
(32) Li, J. J.; Li, Q.; Wang, Z. C.; Deepak, F. L. Real-Time Dynamical Observation of Lattice Induced Nucleation and Growth in Interfacial Solid-Solid Phase Transitions. *Cryst. Growth Des.* **2016**, *16*, 7256−7262.
(33) Li, J. J.; Wang, Z. C.; Deepak, F. L. *In Situ* Atomic-Scale Observation of Droplet Coalescence Driven Nucleation and Growth at Liquid/Solid Interfaces. *ACS Nano* **2017**, *11*, 5590−5597.
(34) Li, J.; Wang, Z.; Deepak, F. L. Direct Atomic-Scale Observation of Intermediate Pathways of Melting and Crystallization in Supported Bi Nanoparticles. *J. Phys. Chem. Lett.* **2018**, *9*, 961−969.
(35) Li, J.; Chen, J.; Wang, H.; Chen, N.; Wang, Z.; Guo, L.; Deepak, F. L. *In Situ* Atomic-Scale Study of Particle-Mediated Nucleation and Growth in Amorphous Bismuth to Nanocrystal Phase Transformation. *Adv. Sci.* **2018**, *5*, 1700992.
(36) Li, Y.; Zang, L.; Li, Y.; Liu, Y.; Liu, C.; Zhang, Y.; He, H.; Wang, C. Photoinduced Topotactic Growth of Bismuth Nanoparticles from Bulk $SrBi_2Ta_2O_9$. *Chem. Mater.* **2013**, *25*, 2045−2051.
(37) Chung, S.-Y.; Kim, Y.-M.; Kim, J.-G.; Kim, Y.-J. Multiphase Transformation and Ostwald's Rule of Stages During Crystallization of a Metal Phosphate. *Nat. Phys.* **2009**, *5*, 68−73.
(38) Aaronson, H. I. Mechanisms of the Massive Transformation. *Metall. Mater. Trans. A* **2002**, *33*, 2285−2297.
(39) Li, Y.; Chen, G.; Wang, Q.; Wang, X.; Zhou, A.; Shen, Z. Hierarchical ZnS-In_2S_3-CuS Nanospheres with Nanoporous Structure: Facile Synthesis, Growth Mechanism, and Excellent Photocatalytic Activity. *Adv. Funct. Mater.* **2010**, *20*, 3390−3398.
(40) Kowalczyk, P. J.; Mahapatra, O.; McCarthy, D. N.; Kozlowski, W.; Klusek, Z.; Brown, S. A. STM and XPS Investigations of Bismuth Islands on HOPG. *Surf. Sci.* **2011**, *605*, 659−667.
(41) Tolbert, S. H.; Herhold, A. B.; Brus, L. E.; Alivisatos, A. P. Pressure-Induced Structural Transformations in Si Nanocrystals: Surface and Shape Effects. *Phys. Rev. Lett.* **1996**, *76*, 4384−4387.
(42) Horcas, I.; Fernández, R.; Gómez-Rodríguez, J. M.; Colchero, J.; Gómez-Herrero, J.; Baro, A. M. WSXM: a software for scanning probe microscopy and a tool for nanotechnology. *Rev. Sci. Instrum.* **2007**, *78*, 013705.
(43) McCarthy, D. N.; Robertson, D.; Kowalczyk, P. J.; Brown, S. A. The Effects of Annealing and Growth Temperature on the Morphologies of Bi Nanostructures on HOPG. *Surf. Sci.* **2010**, *604*, 1273−1282.
(44) Jeffrey, C. A.; Zheng, S. H.; Bohannan, E.; Harrington, D. A.; Morin, S. X-ray Characterization of As-Deposited, Epitaxial Films of Bi(012) on Au(111). *Surf. Sci.* **2006**, *600*, 95−105.
(45) Cao, C. R.; Lu, Y. M.; Bai, H. Y.; Wang, W. H. High surface mobility and fast surface enhanced crystallization of metallic glass. *Appl. Phys. Lett.* **2015**, *107*, 141606.
(46) Kellermann, G.; Craievich, A. F. Melting and Freezing of Spherical Bismuth Nanoparticles Confined in a Homogeneous Sodium Borate Glass. *Phys. Rev. B: Condens. Matter Mater. Phys.* **2008**, *78*, 054106.
(47) Tan, P.; Xu, N.; Xu, L. Visualizing Kinetic Pathways of Homogeneous Nucleation in Colloidal Crystallization. *Nat. Phys.* **2014**, *10*, 73−79.
(48) Peng, Y.; Wang, F.; Wang, Z.; Alsayed, A. M.; Zhang, Z.; Yodh, A. G.; Han, Y. Two-Step Nucleation Mechanism in Solid−Solid Phase Transitions. *Nat. Mater.* **2015**, *14*, 101−108.

DOI: 10.1021/acs.cgd.8b00370
Cryst. Growth Des. 2018, 18, 5808−5815